Multistatic lidar profiling of urban atmospheric aerosols

E. J. Novitsky and C. R. Philbrick

Department of Electrical Engineering, Pennsylvania State University, University Park, Pennsylvania, USA

Received 1 March 2004; revised 26 June 2004; accepted 3 August 2004; published 18 March 2005.

[1] It has become increasingly important to obtain information on the vertical distribution, i.e., profile, of aerosols in the open atmosphere. To complement data obtained from a monostatic Raman lidar, a multistatic receiver configuration was designed to take measurements of the parallel and perpendicular polarization scattered components for altitudes from 10 m to 1000 m above the ground. The measurements, taken at night, were used to form a polarization ratio that was subsequently fitted using Mie theory and a trimodal lognormal aerosol distribution. Experimental results revealed the presence of strong variations in the aerosol distribution within the nighttime planetary boundary layer with some time sequences revealing rapid temporal and spatial changes. Subsequent modeling of the aerosol profile suggested that the observed aerosol variations may depend on a combination of factors, including altitude, composition, and number density. However, in instances when the atmosphere was found to be uniformly mixed, retrieval of aerosol parameters (number density, median radius, and geometric standard deviation) was obtained.

Citation: Novitsky, E. J., and C. R. Philbrick (2005), Multistatic lidar profiling of urban atmospheric aerosols, *J. Geophys. Res.*, *110*, D07S11, doi:10.1029/2004JD004723.

1. Introduction and Background

[2] This paper discusses the results of data collected by a multistatic lidar configuration during the summer of 2001 in Philadelphia, Pennsylvania, as part of the North-East Oxidant and Particle Study (NE-OPS) sponsored by the United States Environmental Protection Agency (EPA). This study involved a consortium of researchers to investigate air pollution with emphasis on particulates and their evolution in the lower troposphere. Our particular task was to examine the vertical profiles of pollutants and particulate matter in the lower troposphere within the planetary boundary layer [*Novitsky*, 2002]. To overcome the limits that the telescopic form factor imposes on a monostatic lidar's operation in the near field (i.e., low altitudes), three CCD (charge-coupled device) cameras were set up in a line extending from the lidar unit and configured to obtain scattering angle measurements of a particular altitude. By inserting a polarization rotator into the beam, the laser polarization plane was switched (with respect to the cameras' orientation) between parallel and perpendicular polarizations. Remote sensing by a multistatic receiver arrangement has advantages over balloon- and aircraft-mounted instruments in that it can perform continuous measurements in regions that would otherwise be difficult to achieve.

[3] For modeling purposes, this investigation assumed atmospheric aerosols consisted of a trimodal lognormal distribution of homogenous spheres [*Stevens*, 1996; *Whitby et al.*, 1972; *Davies*, 1974; *Kelkar and Joshi*, 1977; *Seinfeld and Pandis*, 1998; *Hobbs*, 1993; *Hobbs et al.*, 1985; *Fitch and Cress*, 1983; *John et al.*, 1990]. The polarization ratio, formed by dividing the observed scattered parallel polarization component by the perpendicular polarization component, was the basis of the theoretical scattering model used in this investigation. It has been shown that using the polarization ratio is a good experimental approach to taking atmospheric scattering measurements since the ratio reduces nonlinearities across the face of the imaging device and reduces differences due to extinction of signals from different locations along the path [*Novitsky*, 2002; *Philbrick et al.*, 1996; *Stevens*, 1996]. Additionally, the polarization ratio approach retains the characteristics of the underlying scattering theory for scattering from a sphere [*Novitsky*, 2002]. Finally, since we were not operating in artic or desert environments [*Mishchenko et al.*, 1995, 2000], and tests revealed minimal cross-polarization, our use of homogenous spheres in the atmospheric model is justified.

[4] The work presented here was based on foundational work conducted by *Stevens* [1996] at Wallops Island, Virginia, where a single linear diode array was used to image a horizontally directed lidar beam. Since Wallops Island offers a consistently warm, humid marine environment during summer and fall months, Stevens was able to fix his choice of index of refraction due to the relative uniformity of the atmosphere. However, when warm dry air masses were present, Stevens had difficulty in matching the theory to the observed data. There are two notable differences between the work of Stevens and this work. First, because we anticipated greater diversity in particle composition in an urban environment, we did not assume an "effective" index of refraction as Stevens did but allowed the index to vary in an attempt to find a reasonable value.

0148-0227/05/2004JD004723$09.00

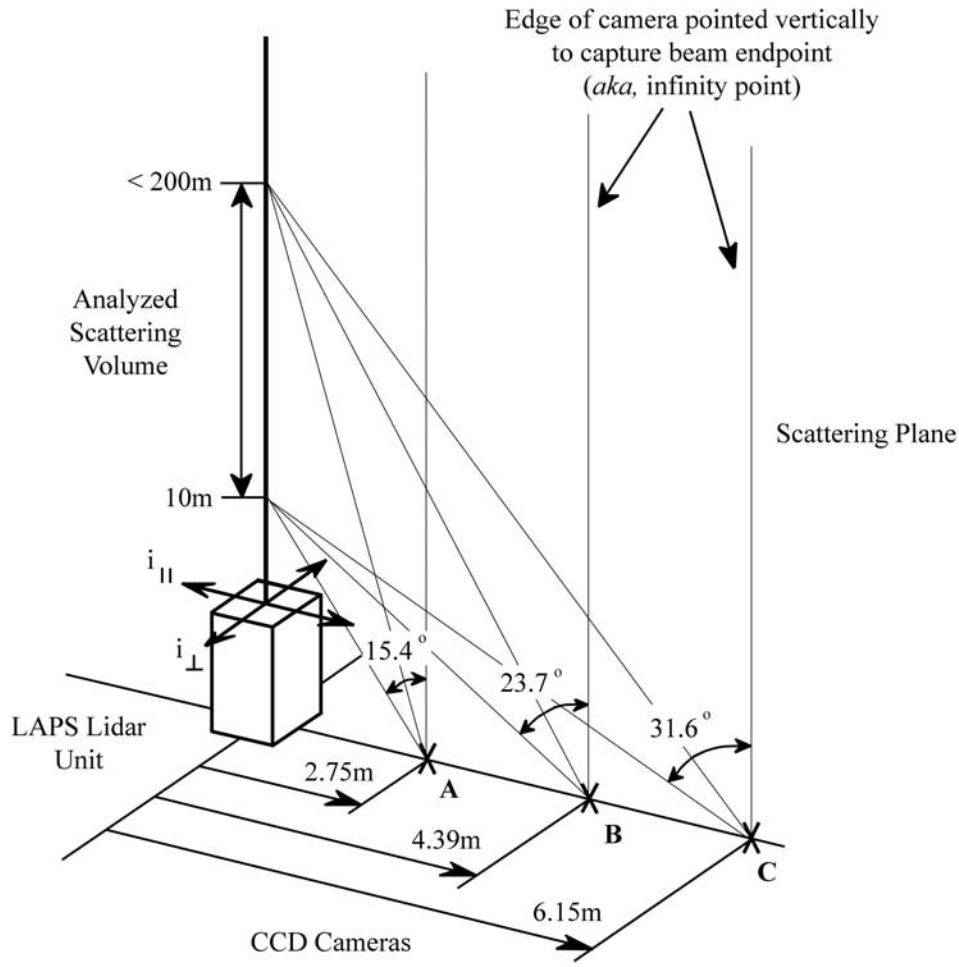

Figure 1. Multistatic receiver equipment and configuration.

Second, three imaging devices were used to obtain sufficient spatial resolution of the vertical path thereby providing additional pieces of independent information with which to perform the inversion process.

[5] Most results of this study showed strong altitude dependence at night within the planetary boundary layer, which complicated our analysis significantly and prevented us from easily obtaining unique particle size density measurements in many cases. However, in situations where the atmosphere was not highly stratified, a reasonable fit between the model and the data was obtained and corroborated with external independent information from other researchers. Additionally, the polarization ratio was demonstrated to be highly sensitive to variations of the real refractive index but insensitive to the imaginary refractive index [*Novitsky*, 2002]. The findings with respect to the complex refractive index are consistent with the underlying theory involving scattering from a sphere [*Bohren and Huffman*, 1983].

2. Experimental Setup and Operation

[6] The basic configuration of the multistatic receiver is shown in Figure 1. Each of the three thermoelectrically cooled cameras (labeled A, B and C) was connected separately to computers. The Lidar Atmospheric Profile Sensor (LAPS) instrument, a Raman lidar that measures profiles of meteorological and air quality properties, provided the necessary illumination at 532 nm. Since the operation of LAPS and its specifics have been thoroughly described elsewhere [*Philbrick*, 2002, 2003], they will not be repeated here.

[7] The basic procedure for operating the multistatic receiver was as follows. Once the cameras were set up, the lidar beam's image was aligned onto each CCD array. A 10 nm interference filter, centered at 532 nm, was also mounted on each camera (the full angular field of view of the cameras was limited 31.8 degrees because of the angular response of the interference filters). The first image taken in a data set was with the polarization of the lidar beam oriented parallel to the scattering plane. The lidar beam polarization was then rotated and a perpendicular polarization image was taken. Finally, using the same integration times as the parallel and perpendicular images, a dark image (with the shutter closed) and a background image (with the laser turned off) were also taken to complete a data set. The dark image is used in the determination of the polarization ratio while the background image is used in the determination of the polarization profiles. Thus, for a given data collection time, twelve images comprise a

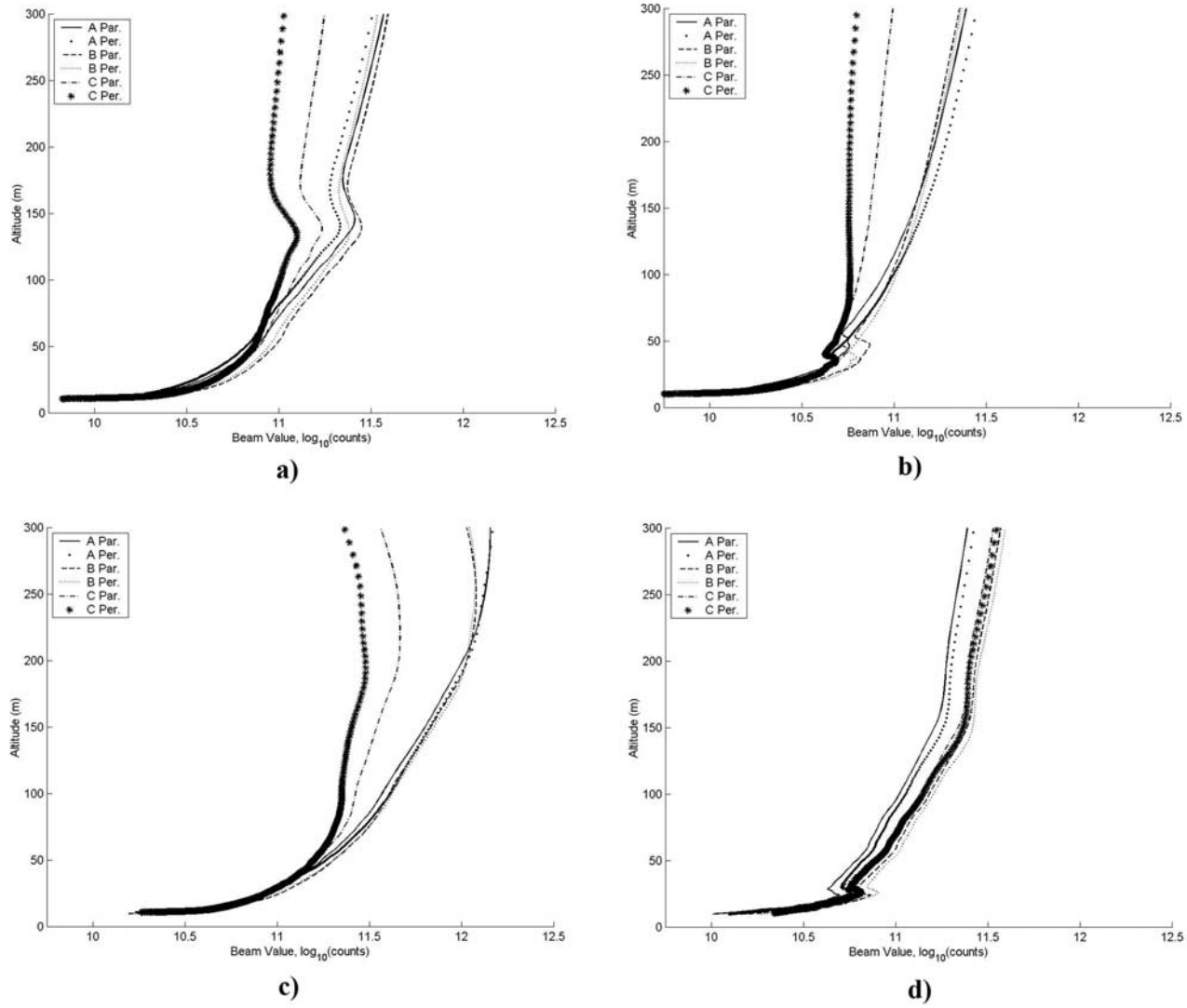

Figure 2. Polarization component profiles from each camera: (a) 7 July 2001, 0257 LT, (b) 13 July 2001, 0230 LT, (c) 23 July 2001, 0350 LT, and (d) 1 October 2001, 0620 LT. See color version of this figure at back of this issue.

data set (four for each camera). The total time between taking parallel and perpendicular images was less than 15 s and a data set was obtained in under 2 min. Further, the integration time for each image was set to 1 s to avoid saturating the 16-bit cameras and to limit the changes observed in the atmosphere.

[8] The polarization ratio was formed from a given camera's data by first subtracting the dark image from each polarization component image and dividing the subsequent results. The use of the ratio of the parallel and perpendicular images significantly reduces the impact of nonlinearities across a camera's imaging array, removes the need to correct for path extinction, and also avoids the need to apply range and volume corrections [*Novitsky*, 2002; *Stevens*, 1996]. Polarization profile images of the perpendicular and the parallel polarization scattering components were obtained by subtracting the background image. Although they were not the primary focus of this effort, the polarization profiles nevertheless provided an important perspective of the measured data.

[9] Characterization of each camera's linear polarization response and image noise was also performed. Because of the thermoelectric coolers, the cameras were found to exhibit very low noise, especially with respect to the typical measured scattering volume, and did not exhibit any measurable linear polarization dependency.

3. Theory and Model

[10] The polarization ratio forms the theoretical foundation of this work and is based on scattering from homogenous spheres [*Bohren and Huffman*, 1983; *Kerker*, 1969]. In mathematical form, the polarization ratio is given by

$$PR(\theta) = \frac{I_{\mathrm{TOTAL}\parallel}(\theta)}{I_{\mathrm{TOTAL}\perp}(\theta)} = \frac{\int |S_2(r,\theta)|^2 y(r) dr + \mathrm{Molecular}_{\parallel}}{\int |S_1(r,\theta)|^2 y(r) dr + \mathrm{Molecular}_{\perp}} \quad (1)$$

where $I_{\mathrm{TOTAL}\parallel}(\theta)$ is total scattering intensity from incident parallel polarization, $I_{\mathrm{TOTAL}\perp}(\theta)$ is total scattering intensity

from incident perpendicular polarization, $|S_{1,2}(r, \theta)|^2$ are scattering matrices (for a given wavelength and index of refraction), and y(r) is the particle size density distribution versus particle radius with units of number per cubic meter (#/m^3). A widely used atmospheric particle distribution is the trimodal lognormal distribution [*Whitby et al.*, 1972; *Davies*, 1974; *Kelkar and Joshi*, 1977; *Seinfeld and Pandis*, 1998; *Aitchison and Brown*, 1957; *Crow and Shimizu*, 1988; *Hobbs*, 1993] given as

$$y(r) = \frac{dN}{d\log r} = \sum_{i=1}^{3} \frac{N_{T_i}}{\sqrt{2\pi}\cdot\log(\sigma_{g_i})} \cdot \exp\left(-\frac{1}{2\log^2(\sigma_{g_i})}\left(\log\left(r/r_{\text{median}_i}\right)\right)^2\right) \quad (2)$$

where the inversion seeks the ith mode's total number density, N_{Ti}, its median radius, $r_{\text{median}i}$, and its geometric standard deviation, σ_{gi}. Last, in (1), the contribution due to the respective molecular component is evident.

[11] Although not explicitly presented in (1), the refractive index is unknown and cannot be neglected or assumed to be some arbitrary value. Investigation of the refractive index's influence on the polarization ratio showed that the real part has a pronounced large-scale effect, while the polarization ratio remains insensitive to the imaginary part over a large range of values. The insensitivity of the polarization ratio to changes in the imaginary part of the refractive index is consistent with the individual polarization components of Mie theory. While the choice of real refractive index will be discussed in the next section, one is cautioned to choose refractive indices that are consistent with observed physical solutions. Thus equation (1) contains 10 unknown parameters (the nine aerosol parameters in equation (2) and the index of refraction), with the scattering angle as the independent variable. Our task is then to measure the polarization ratio and determine a reasonable description of the observed particulate content using the 10 unknown parameters.

4. Observations and Analysis

[12] Data was collected during several nights in Philadelphia in July of 2001. Although the cameras collected data up to 8 km, each individual pixel views an increasing atmospheric volume with increasing altitude, thus preventing credible analysis of the resultant signal of the higher altitudes. Since our primary focus was within the nighttime planetary boundary, the examinations were focused within the first 300 m.

[13] Examples of collected vertical profiles, for each polarization component, taken in July of 2001, are shown in Figure 2. As noted previously, since the profiles are absolute measurements, they have been corrected for range and volume. For comparison, a data set taken in October 2001 in State College, Pennsylvania, has also been included (Figure 2d). Upon inspection of Figures 2a, 2b, and 2d, one notices evidence of atmospheric scattering regions present at altitudes of 140 m, 40 m and 25 m, respectively. These regions are further examined with the use of the polarization ratio. In contrast, Figure 2c shows rather smooth polarization profiles. Shortly, we will discuss Figure 2c as being indicative of a uniformly mixed and stable atmosphere.

[14] Calculation of the polarization ratio provides more information than that obtained from polarization profile plots. Shown in Figures 3 and 4 are the corresponding polarization ratios for the profiles in Figure 2. Immediately, one can see that Figures 3a and 3b, and 4b reveal details of the observed transition layers. The plots that are most useful are those that display the polarization ratio as a function of scattering angle. However, the plots of the polarization ratio versus altitude are also very important in identifying scattering regions. The atmospheric scattering layers of aerosols or atmospheric particulate constituents are revealed in all three sets of plots as features located at the same altitude. Figure 3b shows a scattering transition region at an altitude of approximately 50 m. However, Figure 4a exhibits no separate scattering regions and is an example of a uniformly mixed atmosphere within the planetary boundary layer. Such smooth data was the exception and not the rule as we found many examples where the nighttime planetary boundary exhibited strong altitude dependence in the aerosols present.

[15] During our analysis, questions arose concerning the uniqueness of the solutions. Specifically, is it possible to find a unique solution with so many parameters? In circumstances where there is a strong variation of the aerosols with respect to altitude (e.g., Figures 3a, 3b, and 4b), at a desired altitude, there are only three scattering angle measurements (one measurement for each camera). Thus there is insufficient information to obtain a unique result. However, in situations where the atmosphere is more uniformly mixed (e.g., Figure 4a), retrieval of the aerosol parameters (number density, median radius and geometric standard deviation) may be obtained. Finally, the index of refraction has been found to have a pronounced effect on the polarization ratio [*Novitsky*, 2002] and may significantly affect the values of the retrieved parameters. If one keeps in mind the physical situation atmosphere under observation, then only physical realizable solutions should be tried [*Bohren*, 1986; *Reagan et al.*, 1980]. For example, a good fit of a trimodal lognormal distribution using an index of refraction of 1.75 most likely does not constitute a real physical solution but rather a mathematical one (it is unlikely that all three atmospheric modes should have an index of 1.75 since each mode generally forms under different processes). Thus such a solution is not physically unrealistic. However, in situations where there is large water content, using an overall index of refraction approximately 1.35 in the inversion is possibly justified. Balancing the mathematical and physical aspects of the situation under study can be used to obtain a good solution by rejecting unreasonable results.

[16] In the final analysis, it was found that even when taking into account the physical perspective of the data, one must still retain mathematical justification. An estimation of the relative sensitivity of the polarization ratio due to variations in the 10 aerosol parameters was obtained. From the sensitivity analysis, it was determined that a range of several degrees in the observed scattering data is needed to obtain a well-constrained solution [*Novitsky*, 2002]. Of course, the more one deviates into extreme environments such as desert dusts, no increase of measured scattering angles will suffice since the assumptions of the applied

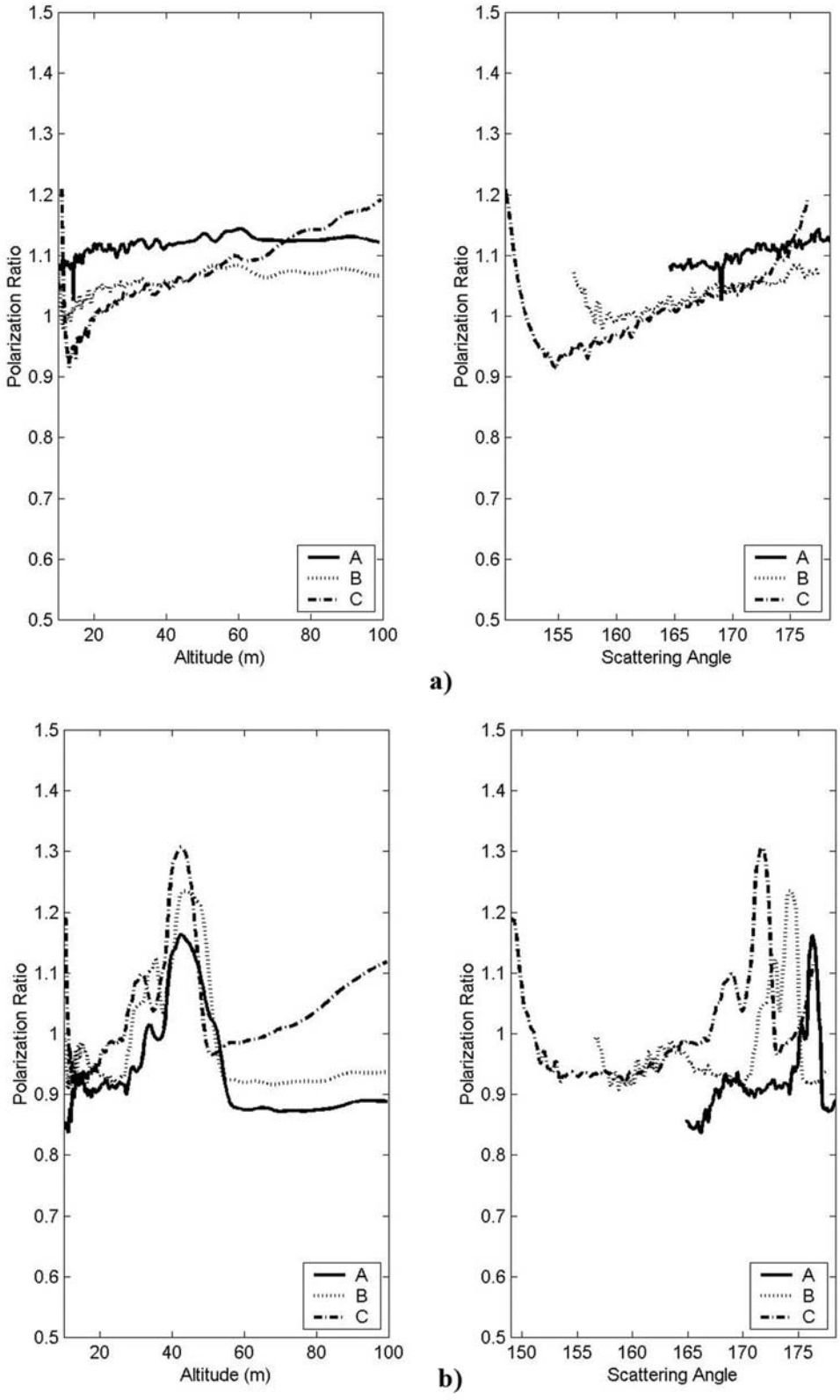

Figure 3. (a and b) Polarization ratios for Figures 2a and 2b, respectively. See color version of this figure at back of this issue.

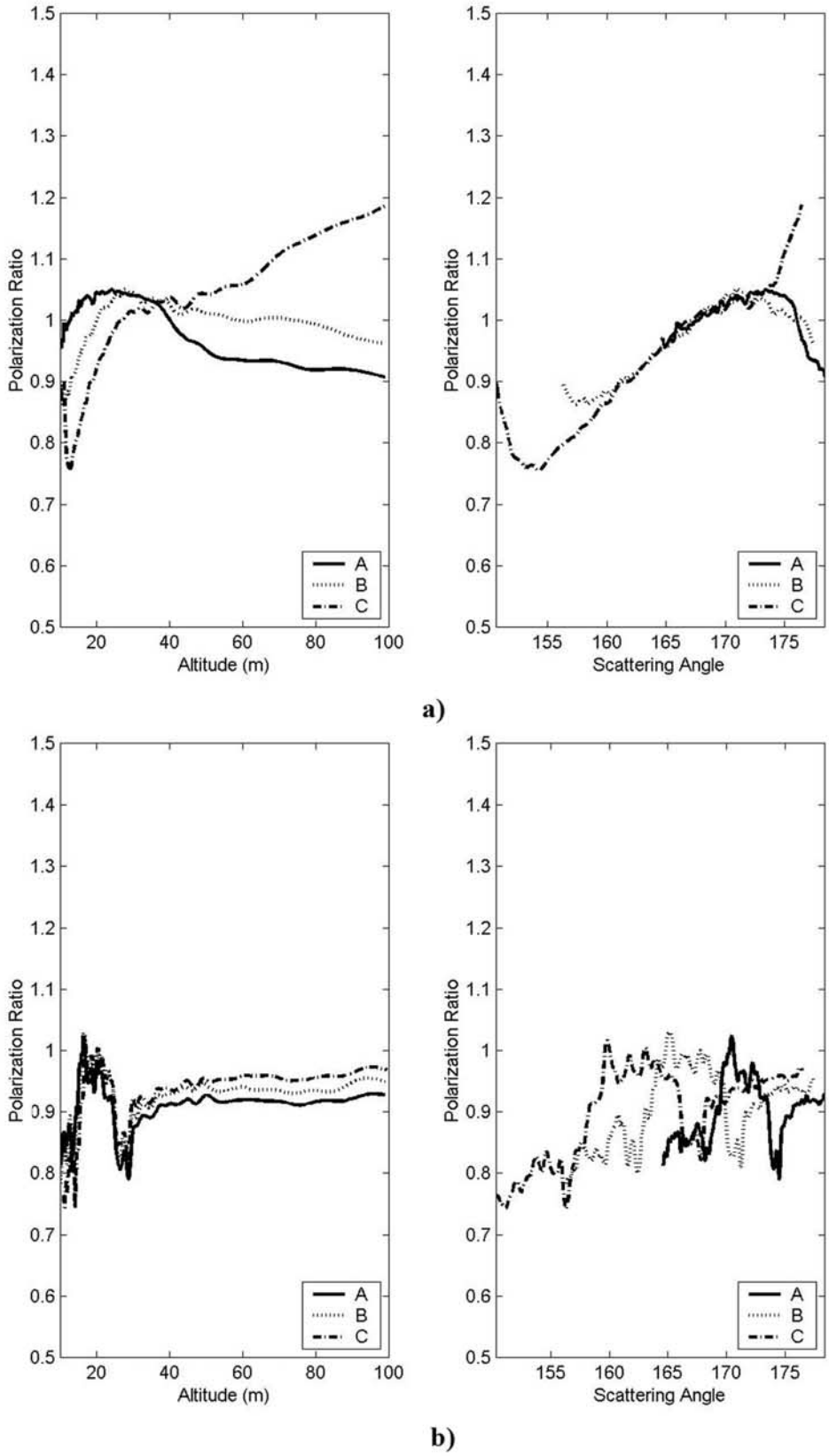

Figure 4. (a and b) Polarization ratios for Figures 2c and 2d, respectively. See color version of this figure at back of this issue.

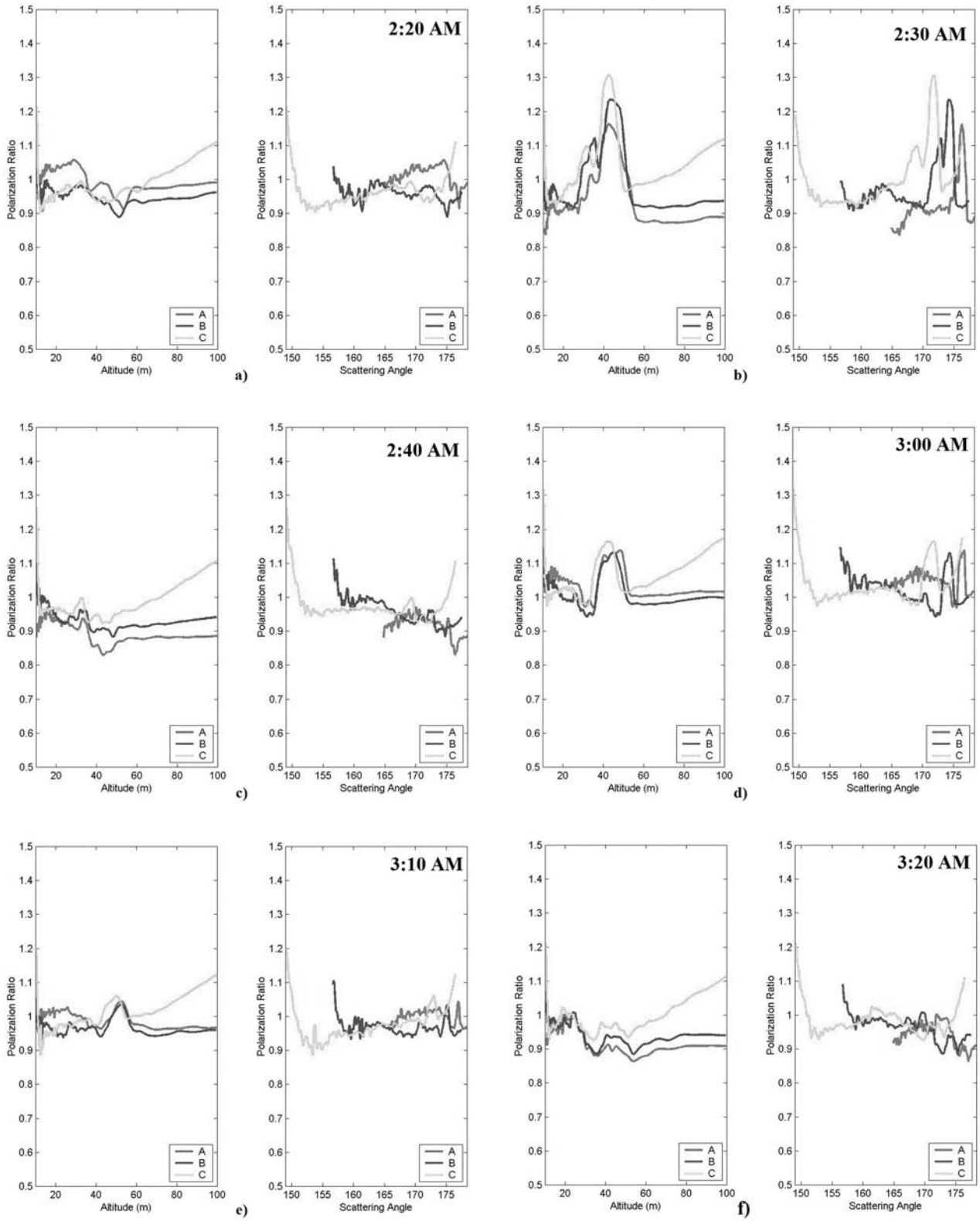

Figure 5. (a–f) Time sequence captured in the early morning of 13 July 2001 (all times are local). Individual plots show polarization ratio versus altitude (left plots) and versus scattering angle (right plots). See color version of this figure at back of this issue.

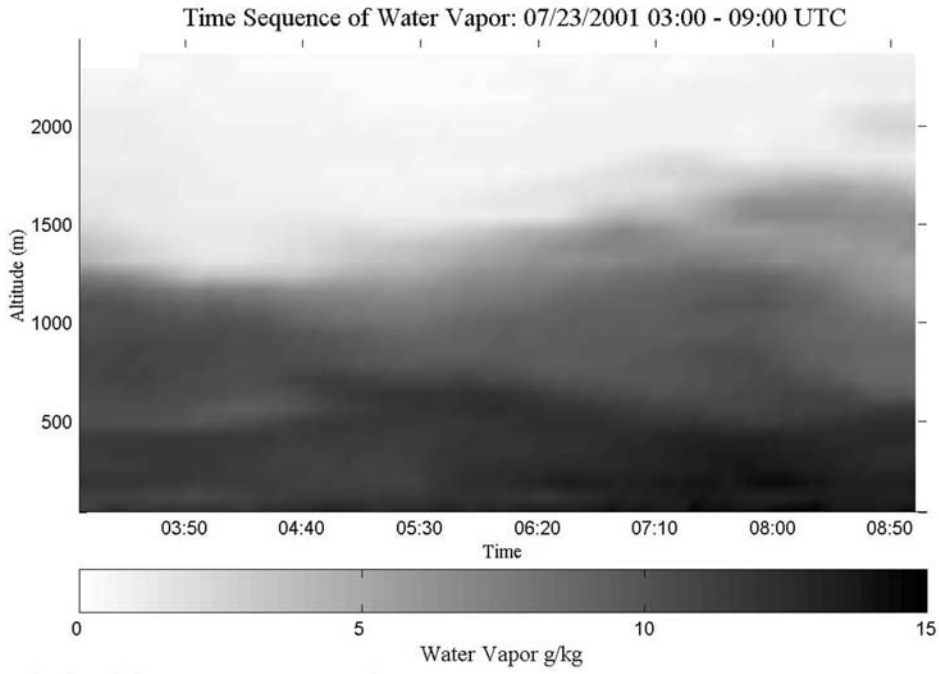

Figure 6. Evolution of water vapor for the given time period of 23 July 2001. See color version of this figure at back of this issue.

theory are violated (nonspherical and/or inhomogenous particles [*Mishchenko et al.*, 1995, 2000]). Further explanation of the polarization sensitivity is beyond the intent of this paper but will be reported at a later date. Additionally, one should avoid using scattering in the backward directions (i.e., scattering angles between 175 and 180 degrees) because the ratio becomes independent of the underlying parameters.

[17] One of the more interesting data sets taken was during the early morning hours of 13 July 2001. As shown in the sequence of Figure 5, a pronounced aerosol layer was observed throughout the night and peaked in size around 0230 local time (LT). No source was attributed to the layer and analysis for its particulate composition could not be adequately obtained with the limited number of scattering angles collected. Since the profile plots showed a marked decrease in scattering intensity (i.e., absorption) within the layer, it was initially thought that the layer might be carbonaceous. However, through some additional modeling, we were able to suggest that the layer may have simply contained a large number of very fine particles, not necessarily composed of carbonaceous material. Thus we were left with an ambiguity that is unresolved without additional independent information. Scattering properties between vertically distributed particle distributions and changes in particle size densities can produce the same measured result.

[18] Although many data sets exhibited strong altitude dependence and hence could not be inverted adequately with just the three camera locations, several instances were obtained that revealed a uniformly mixed atmosphere within the nighttime planetary boundary layer and could be analyzed. The profile of one such instance is shown in Figure 2c and its corresponding polarization ratio shown in Figure 4a. The justification of our hypothesis that the atmosphere at the time of this measurement was uniformly mixed was completed using a variety of independent information. One such piece of information came from our monostatic Raman lidar unit that showed little time variation in the profiles of the water vapor mixing ratio, which was constant throughout this particular time period (see Figure 6). Additionally, instrumented tethered balloons operated by Millersville University showed that mass concentrations at the ground, 100 m, 200 m, and 300 m were all in reasonable agreement and did not exhibit appreciable concentration variations throughout altitude (R. Clark, private communication, 2001). Further, sulfate and carbon measurements taken using ground-based instruments by Harvard's School of Public Health did not show significant levels of these constituents (M. Davey, private communication, 2001). Since the atmosphere on this particular night appeared to be uniformly mixed and contained a uniform distribution of water vapor, ground-based particle number density measurements were used to compare with our inversion analysis. However, one crucial parameter that still remained unknown was the value of the real part of the refractive index of refraction.

[19] Figure 7 shows an example of a fit of the mode to the data using an index of refraction of 1.38, corresponding to a water-based (or wet) aerosol. Here, a significant second aerosol mode could not be justified in our analysis and so it was excluded. This is not to suggest that a second mode does not exist but that the second mode is not strong enough to warrant inclusion in our model simulation of the data as a separate mode. However, the choice of refractive index is admittedly arbitrary and so several reasonable indices from 1.33 to 1.45 were tried. Table 1 summarizes the range of aerosol parameters retrieved in the analysis. The nominal values given are simply the parameters that were found that gave reasonable fits of the model to the data. However, from our investigation of the polarization ratio with respect to

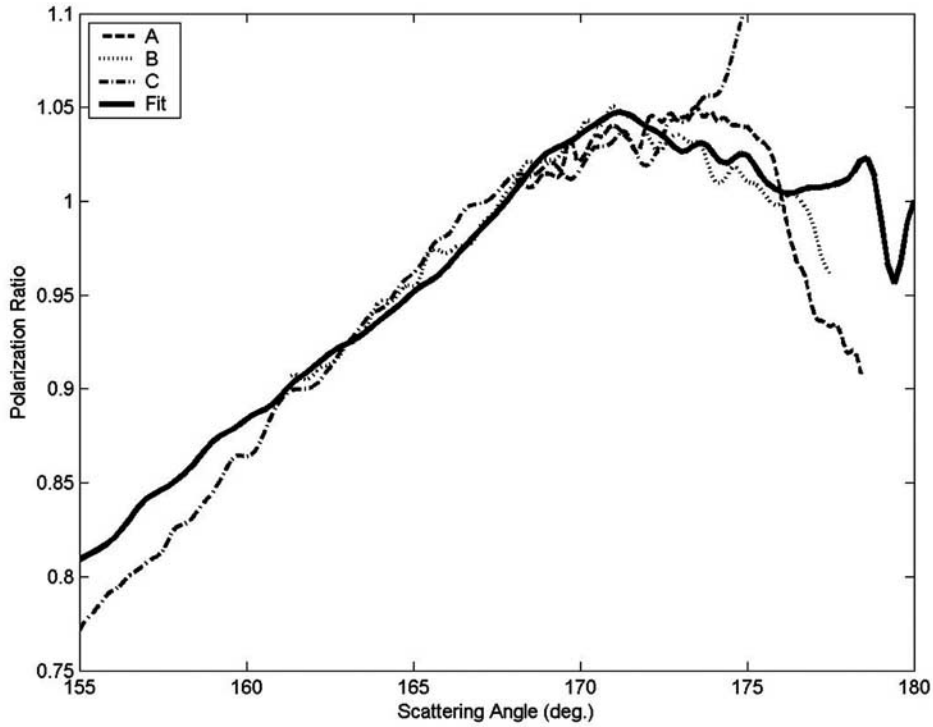

a)

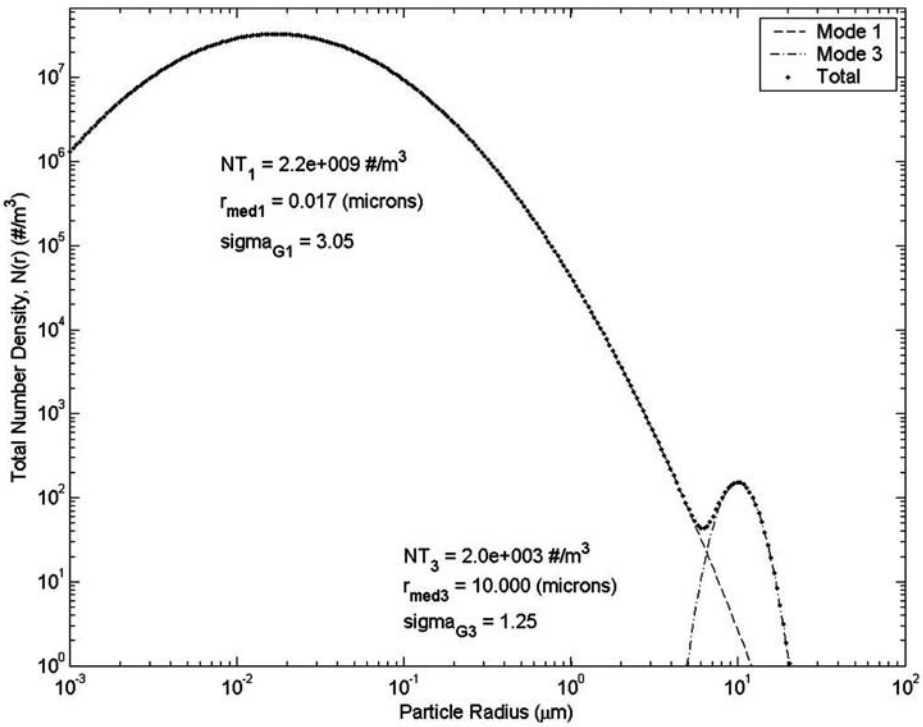

b)

Figure 7. (a) Polarization ratio fit using aerosol parameters listed in Table 1 for an index of 1.38. (b) Corresponding lognormal distribution of total number density versus particle radius. See color version of this figure at back of this issue.

Table 1. Range of Parameters for Polarization Ratio Fit to Data of 0350 LT, 22 July 2001[a]

Index	N_{T1} Nominal (Range), #/m^3	r_{med1} Nominal (Range), nm	σ_{g1} Nominal (Range)	N_{T3} Nominal (Range), #/m^3	r_{med3} Nominal (Range), μm	σ_{g3} Nominal (Range)
1.33	1.1e8 (0.7e8–1.2e8)	11 (9–12)	4.99 (4.65–5.1)	4.5e3 (1e3–6e3)	12 (8–13)	1.4 (1.3–1.55)
1.38	2.2e9 (1.8e9–2.4e9)	17 (15–18)	3.05 (2.95–3.10)	2e3 (1e3–3e3)	10 (9–14)	1.25 (1.15–1.4)
1.40	2.2e8 (1.8e8–2.9e8)	30 (28–33)	3.1 (3.0–3.2)	2e3 (1.5e3–6e3)	10 (9–15)	1.2 (1.1–1.65)
1.44	3.3e7 (2.5e7–3.6e7)	60 (57–62)	2.95 (2.75–3.0)	2e3 (1e3–3e3)	10 (8–12)	1.4 (1.35–1.75)

[a]Read 1.1e8 as 1.1×10^8.

changes in the aerosol parameters, it is more appropriate at this stage to give a range of aerosol parameters. Thus the range of a particular parameter was found by keeping the other parameters set at their nominal value and then varying the desired parameter until the fit of the polarization ratio no longer matched the general trend of the data. It is immediately seen from Table 1 that there can be a wide range in the retrieved parameters, especially with respect to smaller particle sizes and underscores the difficulty in obtaining very accurate aerosol information in the open atmosphere from light scattering measurements.

[20] While it is certainly desirable not to have such a large range in aerosol parameters, the analysis represents the best we can do at this point and, more importantly, it shows where efforts should be focused in the future.

5. Summary

[21] Using a multistatic arrangement consisting of three distinct imaging devices and a monostatic lidar, measurements of nighttime lower tropospheric aerosols were taken in Philadelphia in the summer of 2001. Most measurements revealed the presence of strong, altitude-dependent layers of aerosols within the nighttime planetary boundary layer thereby precluding a more detailed analysis to obtain accurate particle size density information. Further, in situations where the atmosphere was found to be uniformly mixed, the uncertainty of the refractive index yielded a wide range of possible lognormal parameters, particularly for small particle sizes, that could be used to fit the data. However, by using additional information from ground-based sensors, reasonable solutions were obtained for the uniformly mixed atmosphere.

[22] **Acknowledgments.** This work was supported in part by the United States Environmental Protection Agency, grant R826373. The authors also wish to give special thanks to Alex Achey, Gregg O'Marr, and Corey Slick, for their extraordinary efforts toward completing this project.

References

Aitchison, J., and J. A. C. Brown (1957), *The Lognormal Distribution*, 176 pp., Cambridge Univ. Press, New York.

Bohren, C. F. (1986), Applicability of effective-medium theories to problems of scattering and absorption by nonhomogeneous atmospheric particles, *J. Atmos. Sci.*, *43*(5), 468–475.

Bohren, C. F., and D. R. Huffman (1983), *Absorption and Scattering of Light by Small Particles*, 530 pp., John Wiley, Hoboken, N. J.

Crow, E. L., and K. Shimizu (1988), *Lognormal Distributions*, 387 pp., CRC Press, Boca Raton, Fla.

Davies, C. N. (1974), Size distribution of atmospheric particles, *J. Aerosol Sci.*, *5*, 293–300.

Fitch, B. W., and T. S. Cress (1983), Spatial and temporal variations of tropospheric aerosol volume distributions, *J. Clim. Appl. Meteorol.*, *22*, 1262–1269.

Hobbs, P. V. (Ed.) (1993), *Aerosol-Cloud-Climate Interactions*, 233 pp., Elsevier, New York.

Hobbs, P. V., D. A. Bowdle, and L. F. Radke (1985), Particles in the lower troposphere over the high plains of the United States. Part I: Size distributions, elemental compositions and morphologies, *J. Clim. Appl. Meteorol.*, *24*, 1344–1356.

John, W., S. M. Wall, J. L. Ondo, and W. Winklmayr (1990), Modes in the size distributions of atmospheric inorganic aerosols, *Atmos. Environ., Part A*, *24*, 2349–2359.

Kelkar, D. N., and P. V. Joshi (1977), A note on the size distribution of aerosols in urban atmospheres, *Atmos. Environ.*, *11*, 531–534.

Kerker, M. (1969), *The Scattering of Light and Other Electromagnetic Radiation*, 666 pp., Elsevier, New York.

Mishchenko, M. I., A. A. Lacis, B. E. Carlson, and L. D. Travis (1995), Nonsphericity of dust-like tropospheric aerosols: Implications for aerosol remote sensing and climate modeling, *Geophys. Res. Lett.*, *22*(9), 1077–1080.

Mishchenko, M. I., J. W. Hovenier, and L. D. Travis (Eds.) (2000), *Light Scattering by Nonspherical Particles: Theory, Measurements and Applications*, 690 pp., Elsevier, New York.

Novitsky, E. J. (2002), Multistatic lidar profile measurements of lower tropospheric aerosol and particulate matter, Ph.D. thesis, 287 pp., Dep. of Electr. Eng., Pa. State Univ., University Park.

Philbrick, C. R. (2002), Overview of Raman lidar techniques for air pollution measurements, in *Lidar Remote Sensing for Industry and Environment Monitoring II*, *Proc. SPIE Int. Soc. Opt. Eng.*, *4484*, 136–150.

Philbrick, C. R. (2003), Application of Raman lidar advancements in meteorology and air quality monitoring, in *Lidar Remote Sensing for Industry and Environment Monitoring III*, *Proc. SPIE Int. Soc. Opt. Eng.*, *4893*, 61–69.

Philbrick, C. R., M. D. O'Brien, D. B. Lysak, T. D. Stevens, and F. Balsiger (1996), Remote sensing by active and passive optical techniques, in *NATO/AGARD Proceedings on Remote Sensing*, *AGARD Conf. Proc.*, *582*, 8.1–8.9.

Reagan, J. A., D. M. Byrne, M. D. King, J. D. Spinhirne, and B. M. Herman (1980), Determination of the complex refractive index and size distribution of atmospheric particulates from bistatic-monostatic lidar and solar radiometer measurements, *J. Geophys. Res.*, *85*(C3), 1591–1599.

Seinfeld, J. H., and S. N. Pandis (1998), *Atmospheric Chemistry and Physics: From Air Pollution to Climate Change*, 1326 pp., John Wiley, Hoboken, N. J.

Stevens, T. D. (1996), Bistatic lidar measurements of lower tropospheric aerosols, Ph.D. thesis, 247 pp., Dep. of Electr. Eng., Pa. State Univ., University Park.

Whitby, K. T., R. B. Husar, and B. Y. H. Liu (1972), The aerosol distribution of Los Angeles smog, *J. Colloid Interface Sci.*, *39*(1), 177–204.

E. J. Novitsky and C. R. Philbrick, Department of Electrical Engineering, Pennsylvania State University, University Park, PA 16802-2705, USA. (ejn103@psu.edu; crp3@psu.edu)

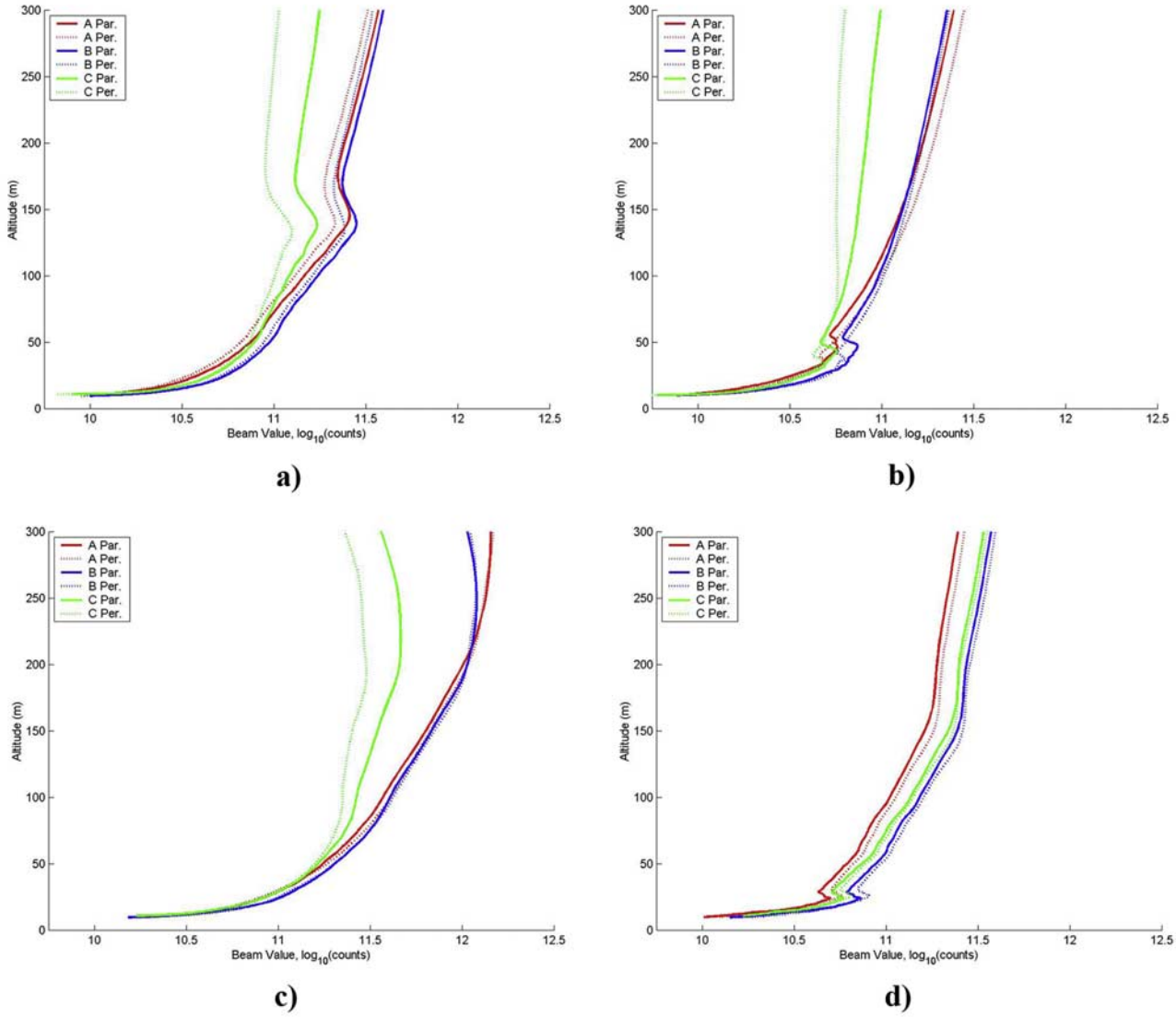

Figure 2. Polarization component profiles from each camera: (a) 7 July 2001, 0257 LT, (b) 13 July 2001, 0230 LT, (c) 23 July 2001, 0350 LT, and (d) 1 October 2001, 0620 LT.

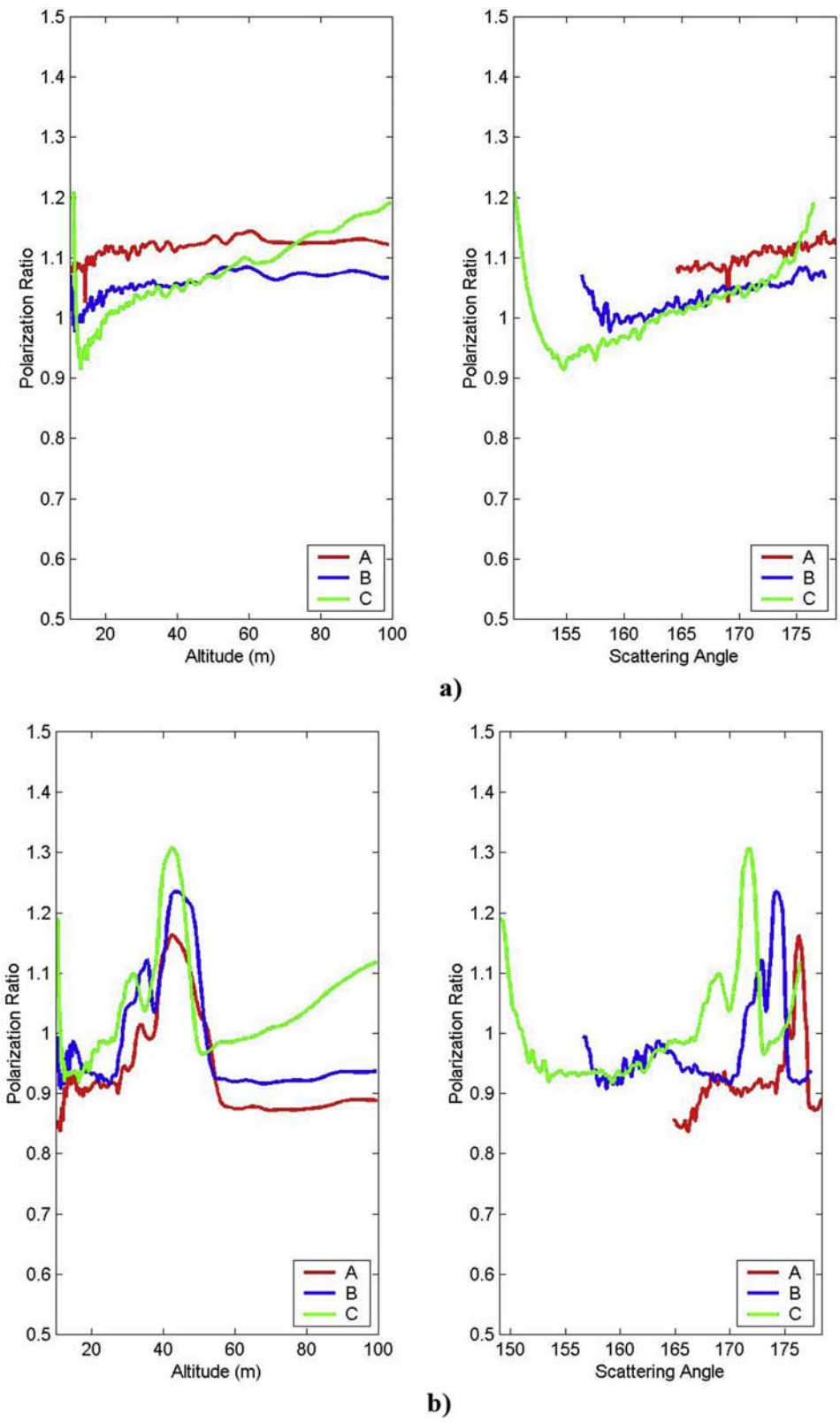

Figure 3. (a and b) Polarization ratios for Figures 2a and 2b, respectively.

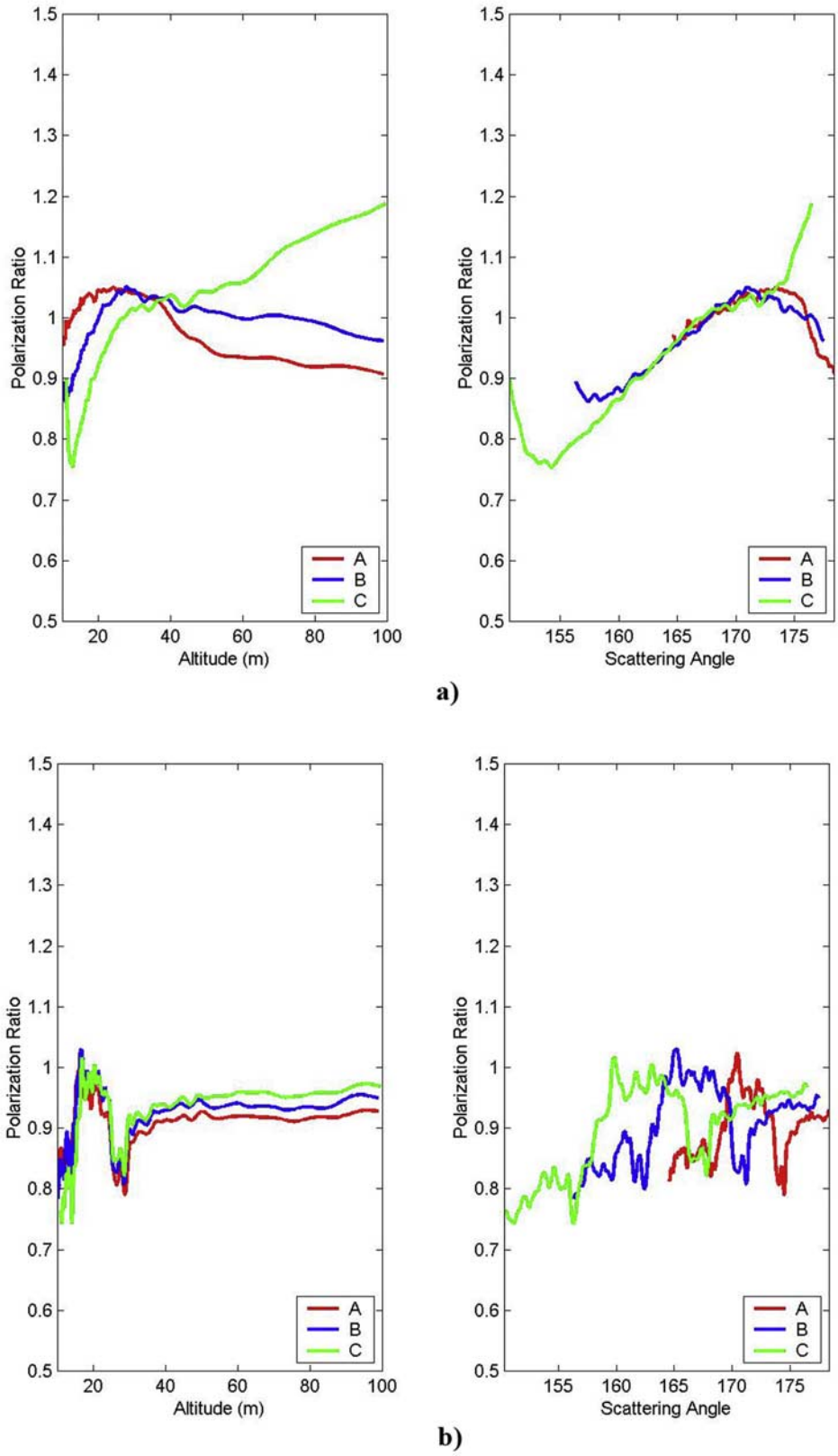

Figure 4. (a and b) Polarization ratios for Figures 2c and 2d, respectively.

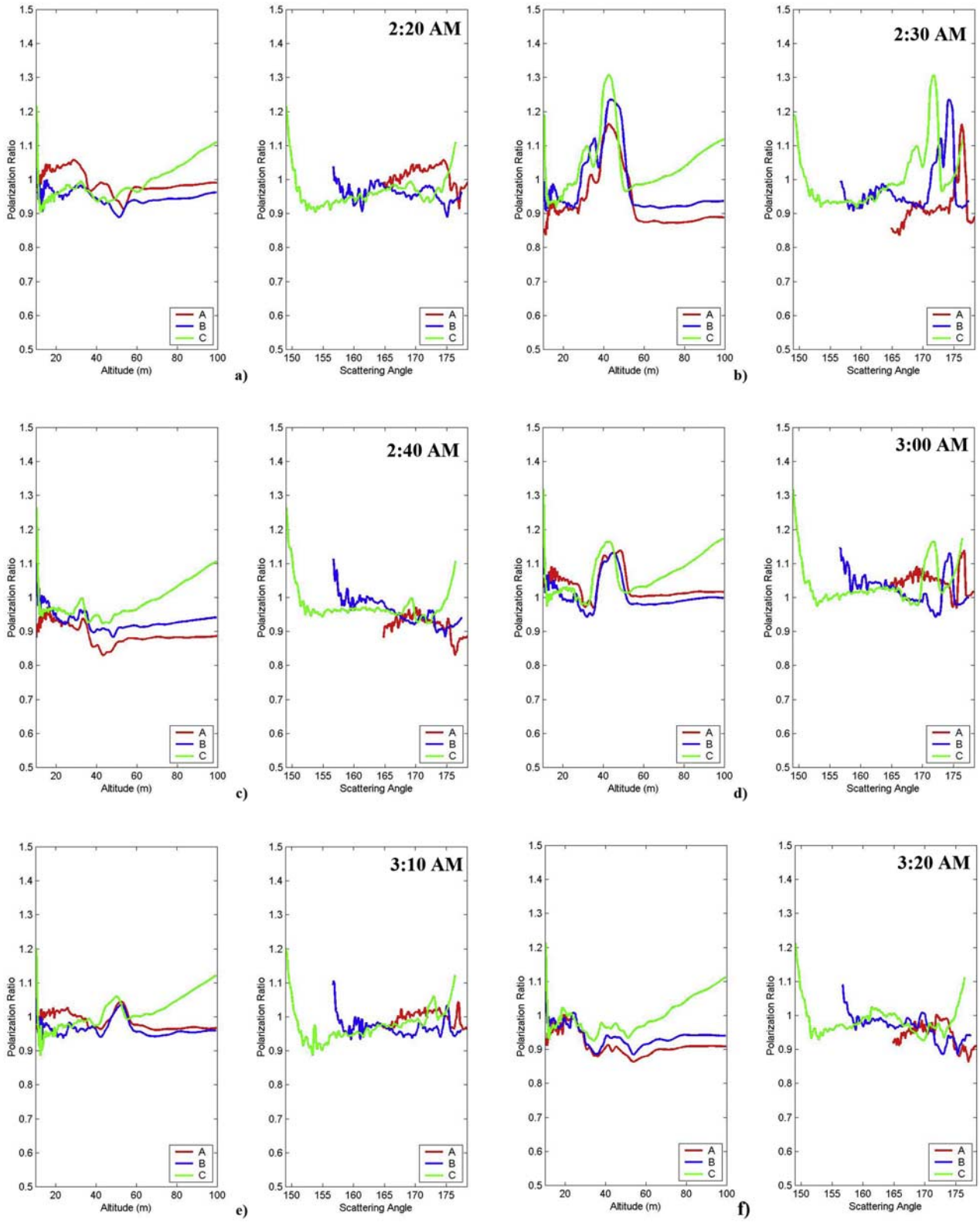

Figure 5. (a–f) Time sequence captured in the early morning of 13 July 2001 (all times are local). Individual plots show polarization ratio versus altitude (left plots) and versus scattering angle (right plots).

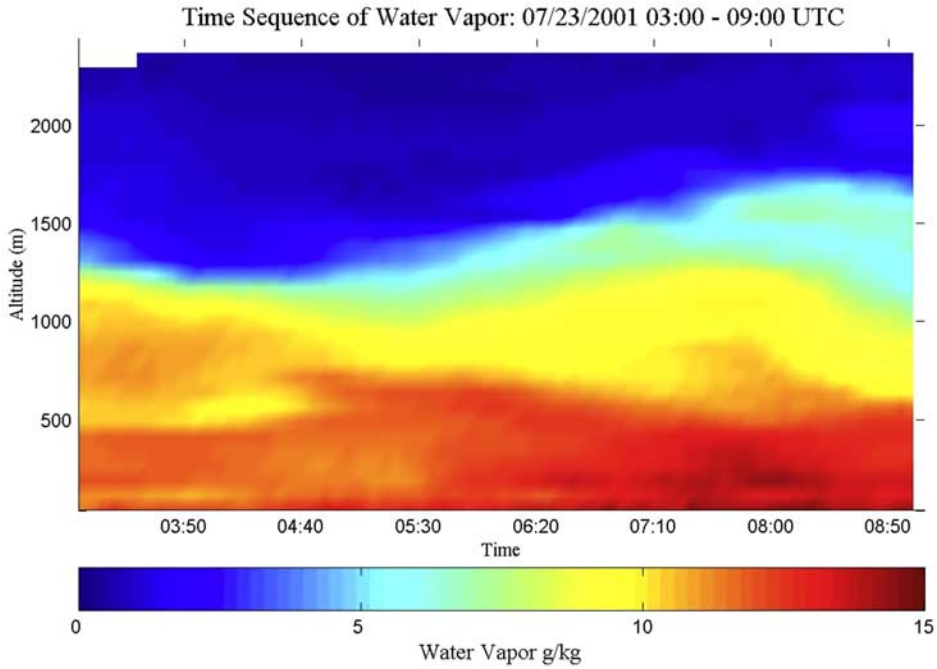

Figure 6. Evolution of water vapor for the given time period of 23 July 2001.

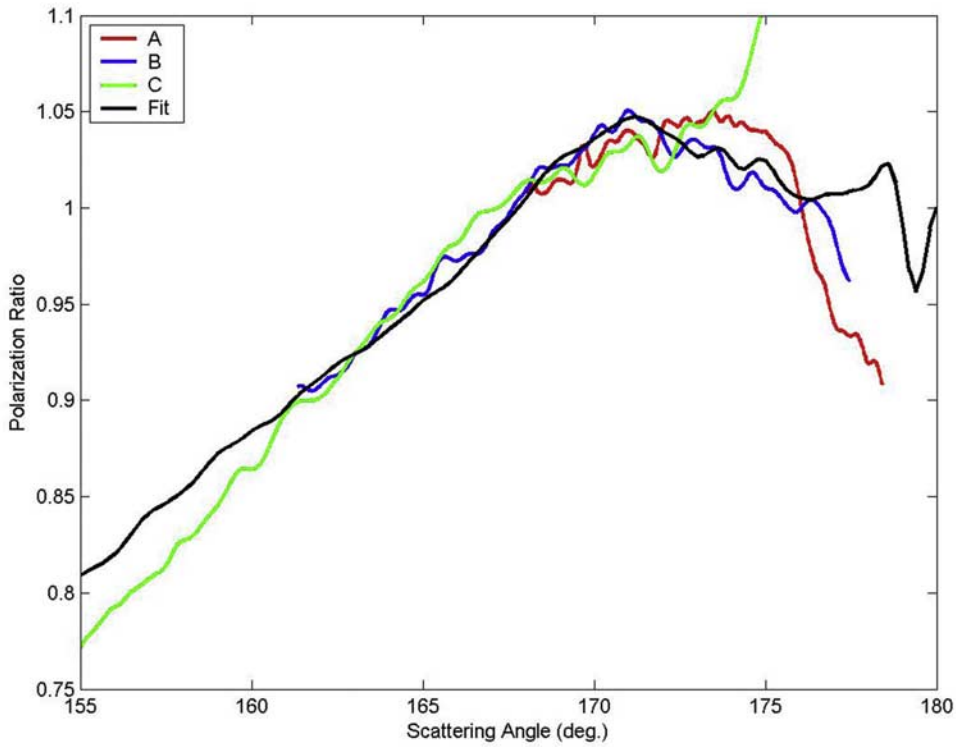

Figure 7. (a) Polarization ratio fit using aerosol parameters listed in Table 1 for an index of 1.38. (b) Corresponding lognormal distribution of total number density versus particle radius.